Multi-layered collagen-based scaffolds for osteochondral defect repair in rabbits.

AUTHOR(S)

Tanya J. Levingstone, Emmet Thompson, Amos Matsiko, Alexander Schepens, John Patrick Gleeson, Fergal O'Brien

CITATION

HANDLE

10779/rcsi.10766900.v1

LICENCE

URL

https://repository.rcsi.com/articles/journal_contribution/Multi-layered_collagen-based_scaffolds_for_osteochondral_defect_repair_in_rabbits_/10766900/1

1   **Multi-Layered Collagen-Based Scaffolds Can Direct Host Stem Cell Differentiation to**

2   **Achieve Osteochondral Defect Repair in Rabbits**

3

4   **Authors:**

5   *Tanya J. Levingstone, BEng, MSc, PhD [1,2,3]

6   *Emmet Thompson, MD, PhD [1,2,3]

7   Amos Matsiko, MEng, PhD [1,2,3]

8   Alexander Schepens, MD[4]

9   John P. Gleeson, BA BAI, PhD, MIEI [1,2,3,5]

10   Fergal J. O'Brien, BA, BAI, PhD, FAS, CEng, FIEI [1,2,3]

11

12   * both authors contributed equally to the work

13

14   **Affiliations:**

15   [1] Tissue Engineering Research Group, Dept. of Anatomy, Royal College of Surgeons in

16   Ireland, 123 St. Stephen's Green, Dublin 2, Ireland.

17   [2] Trinity Centre for Bioengineering, Trinity College Dublin ,Dublin 2, Ireland

18   [3] Advanced Materials and Bioengineering Research (AMBER) Centre, RCSI & TCD

19   [4] Department of Orthopaedic Surgery, AZ Sint-Lucas Hospital, Ghent, Belgium

20   [5] SurgaColl Technologies Ltd., Invent Centre, Dublin City University, Dublin, Ireland.

21

22   **Name of the institution where work was completed:**

23   Royal College of Surgeons in Ireland

24

25

26   **Corresponding Author:**

27   Prof. Fergal O'Brien,

28   Department of Anatomy,

29   Royal College of Surgeons in Ireland,

30   123 St. Stephen's Green,

31   Telephone Number: +353 (0)1-402-2149

32   FAX Number: +353(0)1-402-2355

33   Email:fjobrien@rcsi.ie

34

35   **Abstract:**

36   Identification of a suitable treatment for osteochondral repair presents a major challenge due

37   to existing limitations and an urgent clinical need remains for an off-the-shelf, low cost, one-

38   step approach. A biomimetic approach, where the biomaterial itself encourages cellular

39   infiltration from the underlying bone marrow and provides physical and chemical cues to direct

40   these cells to regenerate the damaged tissue, provides a potential solution. To meet this need,

41   a multi-layer collagen-based osteochondral defect repair scaffold has been developed in our

42   group. The objective of this study was to assess the *in vivo* response to this scaffold and

43   determine its ability to facilitate differentiation of host stem cells in each layer in order to repair

44   osteochondral tissue in a critical-sized defect in a rabbit knee. Multi-layer scaffolds were

45   implanted into critical size (3 x 5mm) osteochondral defects created in the medial femoral

46   condyle of the knee joint of New Zealand white rabbits and compared to an empty control

47   group. Repair was assessed macroscopically, histologically and using micro-CT analysis at 12

48   weeks post implantation. Analysis of repair tissue demonstrated an enhanced macroscopic

49   appearance in the multi-layer scaffold group compared to the empty group. In addition, diffuse

50   host cellular infiltration in the scaffold group resulted in tissue regeneration with a zonal

51   organisation, with repair of the subchondral bone, formation of an overlying cartilaginous layer

52   and evidence of an intermediate tidemark. These results demonstrate the potential of this

53   biomimetic multi-layered scaffold to support and guide the host reparative response in the

54   treatment of osteochondral defects.

Introduction

Cartilage has a limited capacity to regenerate following injury and thus poses a significant clinical problem. Osteochondral defects involving the smooth cartilage lining of the articulating surface and the underlying subchondral bone, are particularly problematic as they frequently occur in young active patients due to diseases such as osteochondritis dissecans, or as a result of traumatic injury to the joint. While some treatment options, such as microfracture, mosaicplasty and autologous chondrocyte implantation (ACI), are available to orthopaedic surgeons, success using these techniques is limited and frequently does not result in long lasting repair of the defect. This can eventually lead to the requirement for joint replacement. Cartilage is avascular and chondrocytes, the cellular components of cartilage, are present in low numbers and have poor mitotic ability. These inherent properties of cartilage tissue contribute significantly to its limited regenerative capacity. Regenerative medicine offers some promise in the area but the identification of a suitable cell source poses a significant challenge in the development of strategies for cartilage repair. Autologous chondrocytes, harvested and expanded prior to implantation into the site of damage, is one commonly used cell source. This approach has a number of associated limitations including, low numbers of suitable cells, *in vitro* de-differentiation, donor-site morbidity, the requirement for a two-step procedure, and high costs. Other potential cell sources are under investigation, including chondrocytes from non-articular sources and MSCs harvested from various locations including the bone marrow, adipose tissue and peripheral blood; however, their use clinically is still limited. An urgent clinical need thus remains for an off-the-shelf, low cost, one-step approach to chondral and osteochondral defect repair. In order to meet this need and overcome the requirement for an external cell source, there is now growing focus on the use of a biomaterials-based approach, where rather than supply cells to the defect site, the ideal biomaterial might encourage the

79   infiltration of cells from the underlying bone marrow and provide physical and biochemical

80   cues to direct these cells to regenerate the damaged tissue [1,2,3].

81

82   A number of biomaterials-based approaches to osteochondral defect repair have emerged in

83   recent years. However, such materials tend to consist of separate cartilage and bone repair

84   scaffolds that are fused together using sutures or biological glues rather than truly addressing

85   the integrated layered structure of osteochondral tissues. In addition, the research focus has

86   been mainly on the chondral region of the defect site and has thus neglected the subchondral

87   bone and calcified cartilage regions. It is now recognised that subchondral bone injury can play

88   an important role in the development and progression of degenerative joint disease [4,5]. Thus

89   regeneration of healthy subchondral bone within the defect site is essential in order to achieve

90   completed repair within an osteochondral defect. The calcified cartilage and tidemark regions

91   of the tissue also play a significant role by providing a stable interface between bone and

92   cartilage and play a critical role in preventing vascular invasion from the subchondral bone into

93   the chondral region which can lead to undesirable bony ingrowth. Until now however, no

94   solution exists that addresses the complex challenge of repairing the cartilage, calcified

95   cartilage and the underlying subchondral bone in osteochondral lesions. To meet this need, a

96   biomimetic multi-layered collagen-based scaffold, has recently been designed and developed

97   within our research group for the repair of osteochondral defects [6,7]. This biomimetic

98   scaffold mimics the stratified composition of native osteochondral tissue by seamlessly

99   integrating three distinct collagen-based layers using a novel iterative layering freeze-drying

100   technique. The result is a multi-layered scaffold consisting of a base layer, previously optimised

101   alone for bone repair [8,9], composed of type I collagen and hydroxyapatite (HA); an

102   intermediate layer composed of type I and type II collagen and HA; and a superficial layer,

103   previously optimised for cartilage repair, composed of type I and type II collagen in addition

104   to the glycosaminoglycan hyaluronic acid (HyA) (Fig. 1). This multi-layered scaffold, is

105   characterised by seamless integration between layers, a high porosity with a highly

106   interconnected pore structure [6]. The extracellular matrix macromolecules and biomechanical

107   properties of this scaffold are designed to direct the differentiation of cells to produce cartilage,

108   calcified cartilage and bone within each region of the scaffold. This scaffold has shown

109   promising results *in vitro* and thus in order to assess its potential for translation into clinical

110   use, assessment *in vivo* in an animal model is required.

111

112   The objective of this study was to assess the *in vivo* response of this biomimetic collagen-based

113   multi-layered scaffold and determine its ability to facilitate the repair of osteochondral tissue

114   in a critical-sized, weight bearing defect in a rabbit knee. The specific aims were to evaluate

115   the scaffold's ability to support host cell infiltration and matrix deposition *in vivo*, and to

116   investigate if the composition and micro-structure will direct cell differentiation within the

117   distinct layers of the scaffold leading to tissue regeneration with a zonal organisation similar

118   to that of native osteochondral tissue i.e. superficial articular cartilage, intermediate calcified

119   cartilage and deep subchondral bone.

120

121   **Materials and Methods**

122   *Multi-layered scaffold fabrication*

123   Multi-layered collagen-based osteochondral scaffolds were fabricated as previously described

124   [6]. Briefly, this involved fabrication of individual collagen-based suspensions for the bone

125   layer, intermediate layer and cartilage layer of the scaffold. The bone layer contains 0.5% (w/v)

126   microfibrillar bovine tendon type I collagen (Col1) (Collagen Matrix Inc., NJ, USA) and 1%

127   (w/v) Hydroxyapatite (HA) powder (Captal 'R' Reactor Powder, Plasma Biotal, UK). The

128   intermediate layer contains type I collagen (Col1), type II collagen (Col2) (Porcine type 2

129   collagen, Biom'up, Lyon, France) in 0.5 M acetic acid and adding HA to give final

130   concentrations of 0.5% (w/v) Col1, 0.5% (w/v) Col2 and 0.2 % (w/v) HA. The cartilage layer

131   consists of 0.125% (w/v) Col1, 0.375% (w/v) Col2 and 0.05% (w/v) HyA. A novel 'iterative

132   layering freeze-drying' process was used to fabricate multi-layered scaffolds [6,7]. Briefly,

133   15.6 ml of the base layer suspension was pipetted into a stainless-steel tray (internal

134   dimensions, 60 mm x 60 mm) before being freeze-dried (Virtis Genesis 25EL, Biopharma,

135   Winchester, UK) at a constant cooling rate of $1°C$ min^{-1} to a final freezing temperature of -

136    $40°C$ [10,11]. Following freeze-drying, the base layer was cross-linked using 1-ethyl-3–3-

137   dimethyl aminopropyl carbodiimide (EDAC)/N-hydroxysuccinimide (NHS) (Sigma–Aldrich,

138   Arklow, Ireland) crosslinking at a ratio of 5:2 M and a 6 mM concentration of EDAC g^{-1} of

139   collagen. The intermediate layer was formed by pipetting 7.8 ml of the intermediate layer

140   suspension on top of the hydrated base layer scaffold and freeze-drying as before. Following

141   rehydration, 15.6 ml of the cartilage layer suspension was pipetted on top of it and freeze-dried

142   using prolonged freezing and drying steps. Following freeze-drying, the porous multi-layered

143   scaffolds were dehydrothermally (DHT) cross-linked in a vacuum oven (VacuCell, MMM,

144   Germany) for 24 hours at a pressure of 0.05 bar and a temperature of $105°C$. Scaffolds were

145   cut to 3.5 mm in diameter using a biopsy punch prior to surgery.

146

147   ***Osteochondral defect creation and multi-layered scaffold implantation in a rabbit knee***

148   *In vivo* assessment was carried out in the rabbit medial femoral condyle model under ethical

149   approval (Trinity College Dublin - Ref:191109) and an animal license granted by the Irish

150   Government Department of Health (Ref: B100/4317). A total of eight skeletally mature (9

151   months old) female New Zealand White rabbits (Centre for Biomedical Science Education,

152   Queens University Belfast, UK) of mean weight 3.2 kg (range 2.8-3.6 kg) were used in the

153   study. Under anaesthetic, animals were positioned on their left side and an incision was made

154 using a medial parapatellar arthrotomy approach and lateral dislocation of the patella to gain

155 access to the femoral condyle. A critical-sized defect, 3 mm diameter full-thickness

156 osteochondral defect was created using a surgical drill (J.B. Tough Dental Ltd., Wicklow,

157 Ireland) on the load-bearing area medial femoral condyle to a depth of 5 mm under constant

158 irrigation (Fig. 2a). Animals were randomly assigned to the empty defect group (n=4) or the

159 multi-layered scaffold group (n=4). In the empty defect group, the defects were left empty with

160 no treatment applied. Defects in the multi-layered scaffold group were treated with a sterile

161 cylindrical multi-layered scaffold press-fitted into the defect until level with the native cartilage

162 surface (Fig. 2b). Scaffolds were hydrated in saline prior to implantation. Animals were housed

163 in individual pens for 5 days post-surgery in order to restrict activity during the initial stages

164 of healing and then transferred to group pens for the remainder of the study. Analgesia and

165 antibiotics were administered for 5 days post-surgery (Carprofen 5mg/kg s/c and Enrofloxacin

166 10 mg/kg s/c pre- and post-surgery). Animals were euthanised at 12 weeks post implantation

167 and the distal femur harvested for further analysis.

168

169 *Macroscopic assessment*

170 The macroscopic appearance of repair tissue in each operative site was blindly assessed by

171 three individuals using the International Cartilage Repair Society (ICRS) cartilage repair

172 assessment tool as shown in Table 1. This tool rates cartilage repair tissue as Grade IV (severely

173 abnormal), Grade III (abnormal), Grade II (nearly normal) or Grade I (normal) based on the

174 degree of defect repair, degree of integration and macroscopic appearance.

175

176 *Microcomputed tomography*

177 Microcomputed tomography (micro CT) was performed on all samples using a Scanco Medical

178 40 Micro CT system (Scanco Medical, Bassersdorf, Switzerland) with 70 kVP X-ray source

179   and 112 µA (resolution of ~12µm). Three-dimensional reconstructions were performed using

180   a threshold of 140 in a scale from 0 – 1000. A volume of interest (VOI) was defined in order

181   to assess healing within the subchondral bone region of the defect site. Repair was expressed

182   as percentage bone volume over total volume (% BV/TV).

183

184   ***Histological analysis***

185   Formalin fixed samples were decalcified using 15% ethylenediaminetetraacetic acid (EDTA,

186   Fluka BioChemika, Sigma-Aldrich), bisected in the longitudinal axis using the lateral border

187   of the intercondylar notch as a guide, and processed using an automated tissue processor

188   (ASP300, Leica, Germany) before being embedded in paraffin wax blocks. Sections (7µm)

189   were cut using a rotary microtome (Microsystems GmbH, Germany) and mounted on poly-L-

190   lysine coated glass slides (Thermo Scientific, Menzel & Co KG, Germany). Sections were

191   stained using Haematoxylin and Eosin (H&E) staining to examine repair tissue morphology,

192   composition and arrangement, cell infiltration, extracellular matrix (ECM) production and

193   scaffold degradation, Toluidine Blue and Safranin-O/Fast green staining, to assess the presence

194   of proteoglycans and glycosaminoglycans and Masson's trichrome staining to identify

195   collagen. Sections were examined microscopically using standard bright-field and polarised

196   light microscopy and digital images captured (Nikon Microscope Eclipse 90i with NIS

197   Elements software v3.06, Nikon Instruments Europe, The Netherlands).

198

199   ***Statistical analysis***

200   Statistical differences between two treatments were assessed by student's paired t-test. Results

201   are reported in figures as mean ± standard deviation and significance was determined using a

202   probability value of $p<0.05$.

203

Results

Clinical observations and macroscopic evaluation

All animals recovered well post-surgery and within 3 days, ambulated freely with no signs of distress or limping for the duration of the study. On opening the joint 12 weeks post-surgery, there was evidence of glossy regenerated tissue similar to the surrounding host tissue in the multi-layered scaffold group (Fig. 3a). There was no evidence of an inflammatory reaction or degenerative change, construct delamination or loss into the joint cavity in the treated joints based on visual assessment at the time of retrieval. Fibrous and necrotic tissue was observed in the defect site of the empty defect group with cartilage-like tissue formation noted at the periphery in some cases; however this tissue showed a lack of continuity with native tissue. Macroscopic evaluation of the repair tissue was carried out using the ICRS cartilage repair assessment tool. Despite intragroup variability, the results showed that multi-layered scaffold treated animals had an average ICRS score of 8.9/12, placing them in the Grade II (nearly normal) category. In comparison, the empty defect group had a lower average ICRS score of 7.1/12 categorising them as a Grade III (abnormal) score (Fig. 3b). Noticeable depressions were observed in the central region of the defect site in the empty defect group. In contrast, improved integration with native tissue was seen in the multi-layered scaffold group with less obvious central depression and less fissuring of the surface.

Microcomputed tomography

The multi-layered scaffold group induced extensive bone repair within the subchondral region of operated knees by 12 weeks post-surgery. Qualitative evaluation of 2D projection images showed that multi-layered scaffold implanted knees showed advanced stages of bone repair (Fig. 4b). Bone formation in the multi-layered scaffold group appears to be adopting a structure similar to that of native bone with denser tissue near the surface adjacent to native cortical

229 bone, overlaying tissue with features of trabecular bone. This regenerated bone remained

230 confined to the subchondral region of operated knees and did not extend above this level into

231 the cartilage region. Quantification of bone formation in the multi-layered scaffold group was

232 found to be significantly greater than that in the empty defect group (Fig. 4c).

233

234 *Histological analysis*

235 Histological analysis was consistent with micro-CT assessment with greater levels of bone

236 formation observed within the defects treated with the multi-layered scaffold group compared

237 to empty defect controls. Despite intragroup variability, major histological differences were

238 demonstrated between multi-layered scaffold and empty defect groups. Adequate healing of

239 the osteochondral defect was not seen in the empty defect group, with all empty defects noted

240 to have deep fissuring, large residual void spaces, subchondral cyst formation, poor bone repair

241 and mainly fibrous tissue formation (Fig. 5a and 6a). Notable findings in the multi-layered

242 scaffold group were the regeneration of bone tissue within the subchondral region and the

243 formation of an overlying cartilage layer (Fig. 5b and 6b). However, some areas of scaffold

244 depression (Fig. 5b), shallow fissuring and areas of fibrocartilage were seen within the multi-

245 layered scaffold group. Polarised light microscopy confirmed that the newly regenerated

246 subchondral bone had already adopted a concentric lamellar pattern seen in mature subchondral

247 trabecular bone by 12 weeks post-surgery (Fig. 6d). No regions of avascular necrosis were

248 observed in the multi-layered scaffold group, although one sample was found to contain a small

249 subchondral cyst (Fig. 5b).

250

251 Cells and matrix were present in all samples in the multi-layered scaffold group indicating that

252 host cells had successfully infiltrated throughout the scaffold post-implantation. By 12 weeks

253 these cells exhibited distinct morphologies depending on their location, gradually transitioning

11

254   from superficial chondrocytes to osteocytes in the deep subchondral bone (Fig. 7a).

255   Furthermore, the presence of an intermediate basophilic tidemark (TM) was also observed

256   between the regenerated cartilage and bone (Fig. 7a). This tidemark signified the limiting line

257   for calcification and vascularisation with no areas of bone or blood vessel formation seen in

258   the cartilage region above this line. Below the tidemark areas with similar appearances to native

259   bone, including neovascularsation were seen (BV) (Fig. 7a). There was continuity between the

260   different regions of regenerate tissue indicating that scaffolds had maintained their internal

261   integrity and resisted interfacial delamination *in vivo*.

262

263   Cells in the superficial region, particularly those located towards the periphery of the

264   implantation site, displayed a rounded morphology and were found residing within lacunae

265   (Fig. 7a and 7b), characteristics typical of chondrocytes in native cartilage. Furthermore, a

266   cellular alignment typical of cartilage and matrix positive for glycosaminoglycans was also

267   seen in relation to these cells (Fig. 7b). In the intermediate region, collagen fibres at the junction

268   of newly formed cartilage and bone tissue displayed a vertical orientation on polarized light

269   (Fig. 7c). This is similar to that normally seen at the calcified cartilage region intervening

270   between subchondral bone and articular cartilage in osteochondral tissue. Furthermore, this

271   region coincided with the basophilic tidemark (Fig. 7c).

272

273   Extensive scaffold replacement was noted with most of the original scaffold material no longer

274   visible. Only small remnants of scaffold were observed within the defect site of one animal

275   (Fig. 7d). The newly formed bone had fully integrated with the surrounding host bone and the

276   original defect boundary was not visible after 12 weeks *in vivo*. Osteon development with

277   Haversian canals, osteocytes and mature lamellar bone was seen embedded within the

278 regenerated matrix of the subchondral region previously occupied by the scaffold base layer

279 (Fig. 7e and 7f).

280

281 **Discussion**

282 Despite numerous advances in the treatment of damage to the articular cartilage, an urgent

283 unmet clinical need remains for an off-the-shelf, low cost, one-step approach to osteochondral

284 defect repair. In order to address this need, a biomimetic multi-layered collagen-based scaffold

285 has been designed within our group for osteochondral defect repair. This highly porous scaffold

286 has previously demonstrated biocompatibility and the potential for cells to attach to and

287 infiltrate through its porous microstructure [6]. The overall aim of this study was to assess the

288 *in vivo* response of this multi-layered scaffold and determine its potential to facilitate the repair

289 of osteochondral tissue in a critical-sized, weight bearing defect in a rabbit knee. Specifically,

290 we investigated the scaffold's ability to support host cellular infiltration and matrix deposition

291 *in vivo* and investigated if the layered arrangement of the scaffold led to tissue regeneration

292 with a zonal organisation similar to that of native osteochondral tissue. Results showed that the

293 scaffold enhanced the macroscopic appearance of the articular surface, as assessed using an

294 ICRS evaluation tool, compared to empty defect controls. Histological analysis showed diffuse

295 cellular infiltration and matrix production throughout the scaffold 12 weeks post-surgery.

296 Staining revealed cartilaginous tissue in the superficial region of the defect site overlying

297 significant new subchondral bone formation, confirmed by micro CT evaluation. Furthermore,

298 a calcified cartilage-like layer was observed between the bone and cartilage layers and was

299 associated with a newly formed tidemark.

300

301 The multi-layered scaffold facilitated host cell infiltration resulting in construct cellularisation,

302 neotissue formation and enhanced healing. The highly porous and highly interconnected pore

13

303   structure of the multi-layered scaffold has previously been shown to support cellular infiltration

304   and proliferation *in vitro* [6] and the results reported here demonstrate its ability to permit host

305   cell infiltration *in vivo*. The scaffold rapidly absorbed blood and bone marrow immediately

306   post-implantation as evidenced by the change in colour of the scaffold from white to red (Fig.

307   2b). Histological assessment showed that host cells were able to homogeneously distribute

308   throughout the scaffold. This thus confers a major advantage over cell-based repair techniques

309   that require at least two surgeries with prolonged intervening *in vitro* cultivation periods to

310   ensure cellularisation prior to implantation [12]. Therefore, the multi-layered scaffold

311   investigated herein, might allow for a one-step operative approach, reducing both the surgical

312   and economic burden [13]. Additionally, this scaffold relies purely on its composition and

313   biostructural and biomechanical properties to achieve this response thus negating the

314   requirement for additional biomolecules that have shown some success in other recent

315   investigations [14,15,16,17].

316

317   Macroscopic differences evident in the superficial cartilage region of the defects indicated the

318   benefit of the multi-layered scaffold in promoting cartilage regeneration *in vivo*. Blinded

319   macroscopic assessment of retrieved samples revealed that the multi-layered scaffold group

320   had a Grade II (8.9/12) score (nearly normal) using the ICRS cartilage repair assessment tool

321   (Fig. 3b). It has recently been used in the assessment of cartilage repair techniques used to treat

322   cartilage defects in young competitive athletes which demonstrated that higher scores were

323   consistent with return to preoperative activity including competitive sport [18,19]. The

324   presence of surface depression and fissuring of repair tissue were observed and may be relate

325   to pressure from synovial fluid within the joint. Furthermore, one sample was found to have

326   developed a small subchondral cyst, similar to findings previously reported and attributed to

327   such synovial fluid pressures [20,21,22].

328

329   Histological evaluation showed that infiltrating cells appeared to adopt region specific

330   morphologies including characteristics typical of chondrocytes (Fig. 7a and 7b) and osteocytes

331   (Fig. 7e) in cartilage and bone regions respectively. Following implantation, host cells were

332   absorbed into this hydrophilic collagen-based scaffold and adhered to individual struts within

333   the different scaffold layers. The layer-specific mechanical and compositional properties of

334   these struts likely played a role in guiding host cell differentiation towards a chondrogenic

335   lineage in the type II collagen-hyaluronic acid superficial layer or an osteogenic lineage in the

336   collagen-HA base layer, thus allowing independent but simultaneous tissue formation in each

337   region. It is recognised that the mechanical properties [23,24,25] and composition

338   [26,27,28,29,30,31,32] of a substrate can affect cell differentiation *in vitro*. Specifically, the

339   chondrogenic properties of type II collagen and hyaluronic acid have previously been

340   demonstrated [26,27,28] and the addition of hydroxyapatite to highly porous collagen-based

341   scaffold has been shown to improve their osteogenic [29,30] and osteoinductive properties

342   [31,32]. Given that differences in compressive modulus have previously been observed

343   between the layers of this scaffold[6], it is likely that these differences influenced host cell

344   response and tissue formation following *in vivo* implantation. Furthermore, quantitative

345   assessment demonstrated the potential of this scaffold to promote a significantly higher level

346   of bone formation *in vivo* compared to controls (Fig. 4) and showed that the regenerated bone

347   remained confined to the subchondral region.

348

349   The inclusion of a calcified cartilage region within the multi-layered scaffold and the formation

350   of a tidemark prevented the migration of subchondral bone and vasculature towards the joint

351   surface. The natural boundary between vascularised subchondral bone and avascular articular

352   cartilage at the chondro-osseous junction is the tidemark, found on the superior aspect of the

353   calcified cartilage layer [33]. Upward migration of subchondral bone has been reported in

354   between 25-34% of patients post-ACI [34,35] and *in vivo* assessments of grafts for

355   osteochondral lesion repair have previously failed to spatially restrict bone and vessel growth

356   to the subchondral region following intra-articular implantation [36]. In such an event, direct

357   bone-on-cartilage contact between an ossified graft and the opposing host articular surface

358   within a dynamic joint could cause chondral damage and early progression towards

359   degenerative change [37]. Several interventions have attempted to prevent bone and vessel

360   overgrowth by employing physical or chemical barriers to compartmentalise tissue formation

361   and prevent bone growth in the superficial zone [38,39]. However, in this current study the

362   inclusion of a calcified cartilage region within the multi-layered scaffold and the formation of

363   a tidemark, (Fig. 7a), signified the limiting line for calcification and vascularisation. This is

364   very encouraging and resulted in bone and vessel formation being restricted to the subchondral

365   region (Fig. 7c), thus maintaining an unmineralised avascular cartilage layer.

366

367   The press-fit implantation method used enabled the scaffold to be maintained securely within

368   the defect site allowing for its degradation and replacement with newly formed bone and

369   cartilage. Previous studies have observed difficulties with achieving integration between

370   implants and native tissue [40,41] and in achieving a balance between scaffold degradation and

371   tissue formation [42]. Other natural polymer scaffolds for osteochondral repair have failed to

372   adequately degrade and integrate with host tissues resulting in poor defect healing [37].

373   Therefore, the biomimetic composition of the multi-layered scaffold may have facilitated

374   enhanced integration at interface regions between the neotissue formed and host tissue.

375   Histological analysis also demonstrated that apart from small remnants of one scaffold, all

376   scaffolds had been replaced with nascent bone and cartilage tissue (Fig. 7d). Additionally, the

377   seamless integration of layers within the multi-layered scaffold was maintained *in vivo*.

378 Layered scaffolds have previously been fabricated from individual layers that were

379 subsequently bonded together using agents such as fibrin glue [43,44].This approach presents

380 potential disadvantages as the bonding agents may inhibit cellular infiltration between layers

381 [45].The iterative fabrication process used here achieves strong adherence between layers that

382 has been shown to maintain layer interconnectivity during mechanical testing *in vitro* [6].

383 Furthermore, the *in vivo* assessment carried out in this study suggests its ability to maintain its

384 continuity during unrestricted joint movement over the experimental period.

385

386 Overall, this study demonstrates the *in vivo* proof of concept and significant promise of utilising

387 this multi-layered scaffold for osteochondral defect repair. The rabbit model used is a

388 recommended model for preliminary investigations of devices designed for

389 cartilage/osteochondral repair [46,47,48] and is the most commonly used model for the

390 evaluation of multilayer scaffolds for osteochondral repair [3]. However, in order to further

391 assess the regenerative capacity of the multi-layered scaffold, *in vivo* analysis in larger animal

392 models (caprine and equine) with joints that more closely represent those of humans, is

393 required. While this study has some recognised limitations including small numbers and

394 intragroup variability, the results successfully demonstrate the ability of this biomimetic multi-

395 layered scaffold to support and guide the host reparative response. This approach, when

396 followed by the use of larger animal models, allows for step-wise progression towards

397 translation of new biomaterials to the clinic.

398

399 **Conclusions**

400 In conclusion, this study demonstrates the successful *in vivo* application of a collagen-based

401 multi-layered osteochondral defect repair scaffold in a critical-sized defect in a rabbit knee.

402 The scaffold extracellular matrix macromolecules and biomechanical properties are designed

403 to provide an ideal environment for cell attachment and proliferation and to direct the

404 differentiation of cells to produce cartilage, calcified cartilage and bone within each region of

405 the scaffold. Greater levels of repair were observed in the multi-layer scaffold group compared

406 to the empty group at 12 weeks post implantation. The results demonstrate that diffuse host

407 cellular infiltration in the multi-layered scaffold group resulted in tissue regeneration with a

408 zonal organisation, with repair of the subchondral bone, formation of an overlying cartilaginous

409 layer and evidence of an intermediate tidemark. Overall, these results show the potential of this

410 biomimetic multi-layered scaffold to support and guide the host reparative response in the

411 treatment of osteochondral defects.

412

418

419 **Conflict of Interest**

420 Authors John P Gleeson and Fergal J O'Brien hold IP with a commercial product of related

421 composition to the collagen-based scaffolds used in this study.

422

423 **References**

424 1. M. Keeney, A. Pandit. The osteochondral junction and its repair via bi-phasic tissue

425 engineering scaffolds. Tissue Eng Part B. 15 (2009) 55-73.

426   2. S.P. Nukavarapu, D.L. Dorcemus. Osteochondral tissue engineering: current strategies and

427   challenges. Biotechnol Adv. 31(2013) 706-21.

428   3. J.E. Jeon, C. Vaquette, T.J. Klein, D.W. Hutmacher. Perspectives in multiphasic

429   osteochondral tissue engineering. Anat Rec. 297 (2014) 26-35.

430   4. A. Lahm, P.C. Kreuz, M. Oberst, J. Haberstroh, M. Uhl,. D. Maier. Subchondral and

431   trabecular bone remodeling in canine experimental osteoarthritis. Arch Orthop Trauma Surg.

432   126 (2006) 582-7.

433   5. E.H. Mrosek, A. Lahm, C. Erggelet, M. Uhl, H. Kurz, B. Eissner, J.C. Schagemann.

434   Subchondral bone trauma causes cartilage matrix degeneration: an immunohistochemical

435   analysis in a canine model. Osteoarthr Cartilage. 14 (2006) 171-8.

436   6. T.J. Levingstone, A. Matsiko, G.R. Dickson, F.J. O'Brien, J.P. Gleeson. A biomimetic multi-

437   layered collagen-based scaffold for osteochondral repair. Acta Biomater. 10(5) (2014) 1996-

438   2004.

439   7. J.P. Gleeson, T.J. Levingstone, F.J. O'Brien. Layered scaffold suitable for osteochondral

440   defect repair. Patent WO2010/084481, 2009.

441   8. J.P. Gleeson, N.A. Plunkett, F.J. O'Brien. Addition of hydroxyapatite improves stiffness,

442   interconnectivity and osteogenic potential of a highly porous collagen-based scaffold for bone

443   tissue regeneration. Eur Cell Mater. 20 (2010) 218-30.

444   9. F.G. Lyons, J.P. Gleeson, S. Partap, K. Coghlan, F.J. O'Brien. Novel microhydroxyapatite

445   particles in a collagen scaffold: a bioactive bone void filler? Clin Orthop Relat R. 472(4) (2014)

446   1318-1328

447   10. F.J. O'Brien, B.A.Harley, I.V. Yannas, L.J. Gibson. Influence of freezing rate on pore

448   structure in freeze-dried collagen-GAG scaffolds. Biomaterials. 25 (2004) 1077-86.

19

449   11. F.J. O'Brien, B.A. Harley, I.V. Yannas, L.J. Gibson. The effect of pore size on cell adhesion

450   in collagen-GAG scaffolds. Biomaterials. 26 (2005) 433-41.

451   12. M. Brittberg. Cell Carriers as the Next Generation of Cell Therapy for Cartilage Repair A

452   Review of the Matrix-Induced Autologous Chondrocyte Implantation Procedure. Am. J. Sports

453   Med. 38 (2010) 259-1271.

454   13. E. Kon, G. Filardo, B. Di Matteo, F. Perdisa, M. Marcacci. Matrix assisted autologous

455   chondrocyte transplantation for cartilage treatment: A systematic review. Bone Joint Res. 2

456   (2013) 18-25.

457   14. H. Maehara, S. Sotome, T. Yoshii, I. Torigoe, Y. Kawasaki, Y. Sugata, M. Yuasa, M.

458   Hirano, N. Mochizuki, M. Kikuchi, K. Shinomiya, A. Okawa.. Repair of large osteochondral

459   defects in rabbits using porous hydroxyapatite/collagen (HAp/Col) and fibroblast growth

460   factor-2 (FGF-2). J Orthop Res. 28 (2010) 677-686.

461   15. N. Mohan, N.H. Dormer., K.L. Caldwell, V.H. Key, C.J. Berkland, M.S. Detamore.

462   Continuous gradients of material composition and growth factors for effective regeneration of

463   the osteochondral interface. Tissue Eng Part A.17 (2011) 2845-55.

464   16. R. Reyes, A. Delgado, E. Sanchez, A. Fernandez, A. Hernandez, C. Evora. Repair of an

465   osteochondral defect by sustained delivery of BMP-2 or TGF-beta1 from a bilayered alginate-

466   PLGA scaffold. J Tissue Eng Regen Med. 6 (7) (2014) 521-33.

467   17. T. Re'em, F. Witte, E. Willbold, E. Ruvinov, S. Cohen. Simultaneous regeneration of

468   articular cartilage and subchondral bone induced by spatially presented TGF-beta and BMP-4

469   in a bilayer affinity binding system. Acta Biomater. 8 (2012) 3283-3293.

470   18. R. Gudas, A. Gudaite, A. Pocius, A. Gudiene, E. Cekanauskas, E. Monastyreckiene A.

471   Basevicius . Ten-year follow-up of a prospective, randomized clinical study of mosaic

472 osteochondral autologous transplantation versus microfracture for the treatment of

473 osteochondral defects in the knee joint of athletes. Am J Sports Med. 40 (2012) 2499-508.

474 19. G. Panics., L.R. Hangody, E. Baló, G. Vásárhelyi, T. Gál, L. Hangody. Osteochondral

475 autograft and mosaicplasty in the football (soccer) athlete. Cartilage. 3 (2012) 25s-30s.

476 20. A. Getgood, F. Henson, C. Skelton, E. Herrera, R. Brooks, L.A. Fortier, N. Rushton.. The

477 augmentation of a collagen/glycosaminoglycan biphasic osteochondral scaffold with platelet-

478 rich plasma and concentrated bone marrow aspirate for osteochondral defect repair in sheep:

479 A pilot study. Cartilage. 3 (2012) 351-363.

480 21. A. Getgood, S.J. Kew, R. Brooks, H. Aberman, T. Simon, A.K. Lynn, N. Rushton. .

481 Evaluation of early-stage osteochondral defect repair using a biphasic scaffold based on a

482 collagen-glycosaminoglycan biopolymer in a caprine model. Knee, 19 (2012) 422-430.

483 22. F. Benazzo, M. Cadossi, F. Cavani, M. Fini, G. Giavaresi, S. Setti, R. Cadossi, R. Giardino.

484 Cartilage repair with osteochondral autografts in sheep: Effect of biophysical stimulation with

485 pulsed electromagnetic fields. J Orthop Res. 26 (2008) 631-642.

486 23. D.E. Discher, P. Janmey, Y.L. Wang. Tissue cells feel and respond to the stiffness of their

487 substrate. Science. 310 (2005) 1139–1143

488 24. D. Karamichos , R.A. Brown, V. Mudera. Complex dependence of substrate stiffness and

489 serum concentration on cell-force generation. J Biomed Mater Res. A78 (2) (2006) 407-15.

490 25. J.R. Tse and A.J. Engler. Stiffness gradients mimicking *in vivo* tissue variation regulate

491 mesenchymal stem cell fate, PLoS One. 6 (1) (2011) e15978.

492 26. A. Matsiko , T.J. Levingstone, F.J. O'Brien, J.P. Gleeson. Addition of hyaluronic acid

493 improves cellular infiltration and promotes early-stage chondrogenesis in a collagen-based

494 scaffold for cartilage tissue engineering J Mech Behav Biomed Mater. 11 (2012) 41-52.

495   27. G. Ragetly, D.J. Griffon, Y.S. Chung. The effect of type II collagen coating of chitosan

496   fibrous scaffolds on mesenchymal stem cell adhesion and chondrogenesis. Acta Biomater. 6

497   (10) (2010) 3988–97.

498   28. K.Y. Chang, L.H. Hung, I.M. Chu, C.S. Ko, Y.D. Lee. The application of type II collagen

499   and chondroitin sulfate grafted PCL porous scaffold in cartilage tissue engineering. J Biomed

500   Mater Res A. 92 (2010) 712–723.

501   29. J.P. Gleeson, N.A. Plunkett, F.J. O'Brien. Addition of hydroxyapatite improves stiffness,

502   interconnectivity and osteogenic potential of a highly porous collagen-based scaffold for bone

503   tissue regeneration. Eur Cell Mater. 20 (2010) 218–230.

504   30. J.B. Vines, D.J. Lim, J.M. Anderson, H.W. Jun. Hydroxyapatite nanoparticle reinforced

505   peptide amphiphile nanomatrix enhances the osteogenic differentiation of mesenchymal stem

506   cells by compositional ratios. Acta Biomater. 8 (2012) 4053–4063.

507   31. H. Yuan, J.D. De Bruijn, X. Zhang, C.A. Van Blitterswijk, K. De Groot. Use of an

508   osteoinductive biomaterial as a bone morphogenetic protein carrier. J Mater Sci Mater Med.

509   12 (2001)761–766.

510   32. C.M. Murphy, A. Schindeler, J.P. Gleeson, N.Y.C. Yu, L.C. Cantrill, K. Mikulec, L.

511   Peacock , F.J. O'Brien, D.G. Little . A collagen–hydroxyapatite scaffold allows for binding

512   and co-delivery of recombinant bone morphogenetic proteins and bisphosphonates. Acta

513   Biomater. 10 (5) (2014) 2250-8.

514   33. F. Wang, Z. Ying, X. Duan, H. Tan, B. Yang, L. Guo, G. Chen, G. Dai, Z. Ma, L. Yang.

515   Histomorphometric analysis of adult articular calcified cartilage zone. J Struct Biol. 168

516   (2009) 359-65.

517 34. I.J.P. Henderson, D.P. La Valette. Subchondral bone overgrowth in the presence of full-

518 thickness cartilage defects in the knee. Knee. 12 (2005) 435-440.

519 35. T. Minas, A.H. Gomoll, R. Rosenberger, R.O. Royce, T. Bryant. Increased Failure Rate of

520 Autologous Chondrocyte Implantation After Previous Treatment With Marrow Stimulation

521 Techniques. American Journal of Sports Medicine. 37 (2009) 902-908.

522 36. J.M. Coburn, M. Gibson, S. Monagle, Z. Patterson, J.H. Elisseeff. Bioinspired nanofibers

523 support chondrogenesis for articular cartilage repair. Proc Natl Acad Sci. 109 (2012) 10012-7.

524 37. A. Abarrategi, Y. Lopiz-Morales, V. Ramos, A. Civantos, L. Lopez-Duran, F. Marco, J.L.

525 Lopez Lacomba. Chitosan scaffolds for osteochondral tissue regeneration. J Biomed Mater Res

526 A. 95 (2010) 1132-41.

527 38. E.B. Hunziker, I.M. Driesang, C. Saager. Structural barrier principle for growth factor-

528 based articular cartilage repair. Clin Orthop Relat Res. (2001) S182-9.

529 39. E.B. Hunziker, I.M. Driesang. Functional barrier principle for growth-factor-based articular

530 cartilage repair. Osteoarthritis Cartilage. 11 (2003) 320-7.

531 40. D. Schaefer, I. Martin, G. Jundt, J. Seidel, M. Heberer, A. Grodzinsky, I. Bergin, G.Vunjak-

532 Novakovic, L.E. Freed . Tissue-engineered composites for the repair of large osteochondral

533 defects. Arthritis Rheum. 46 (2002) 2524-34.

534 41. C.H. Chang, T.F. Kuo, C.C. Lin, C.H. Chou, K.H. Chen, F.H. Lin, H.C. Liu. Tissue

535 engineering-based cartilage repair with allogenous chondrocytes and gelatin-chondroitin-

536 hyaluronan tri-copolymer scaffold: A porcine model assessed at 18, 24, and 36 weeks.

537 Biomaterials. 27 (2006) 1876-1888.

538 42. D.W. Hutmacher. Scaffolds in tissue engineering bone and cartilage. Biomaterials. 21

539 (2000) 2529-43.

540   43. C. Scotti, D. Wirz, F. Wolf, D.J. Schaefer, V. Burgin, A.U. Daniels, V. Valderrabano,

541   C. Candrian, M. Jakob, I. Martin, A. Barbero. Engineering human cell-based, functionally

542   integrated osteochondral grafts by biological bonding of engineered cartilage tissues to bony

543   scaffolds. Biomaterials. 31 (2010) 2252-9.

544   44. J. Chen, H. Chen, P. Li, H. Diao, S. Zhu, l. Dong, R. Wang, T. Guo, J. Zhao, J. Zhang.

545   Simultaneous regeneration of articular cartilage and subchondral bone *in vivo* using MSCs

546   induced by a spatially controlled gene delivery system in bilayered integrated scaffolds.

547   Biomaterials. 32 (2011) 4793-805.

548   45. B.A. Harley, A.K. Lynn, Z. Wissner-Gross, W. Bonfield, I.V. Yannas, L.J. Gibson. Design

549   of a multiphase osteochondral scaffold III: Fabrication of layered scaffolds with continuous

550   interfaces. J Biomed Mater Res A. 92 (2010) 1078-93.

551   46. ASTM. Standard Guide for *in vivo* Assessment of implantable devices intended to repair

552   or regenerate articular cartilage. American Society for Testing and Materials, 2010.

553   47. C.R. Chu, M. Szczodry, S. Bruno. Animal models for cartilage regeneration and repair.

554   Tissue Eng Part B Rev. 16 (2010) 105-15.

555   48. J.L. Cook, C.T. Hung, K. Kuroki, A.M. Stoker, C.R. Cook, F.M. Pfeiffer, S. L. Sherman,

556   J. P. Stannard. Animal models of cartilage repair. Bone Joint Res. 3 (2014) 89-94.
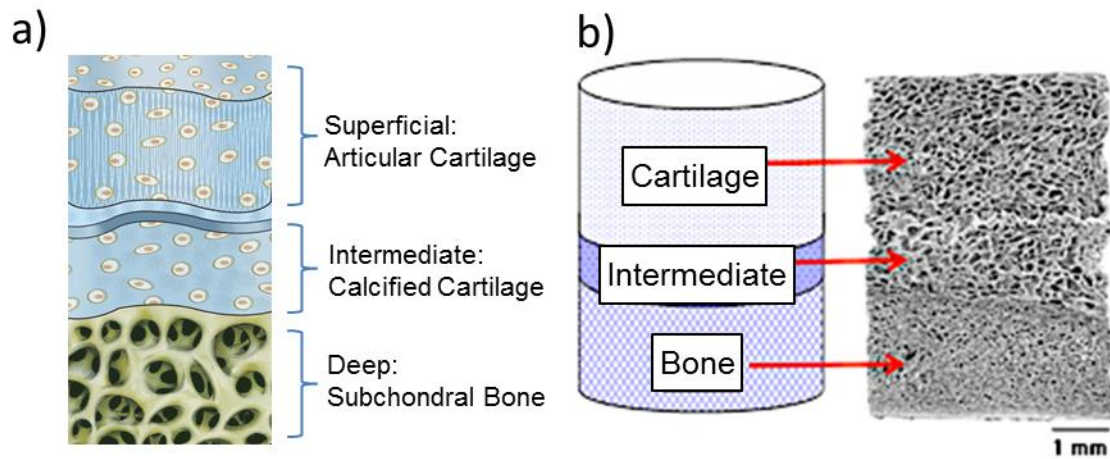
557   **Figures**

Figure 1: Schematic diagrams showing (a) the superficial, intermediate and deep layers of the osteochondral region and (b) the multi-layered scaffold. This scaffold is fabricated using three distinct collagen-based slurries sequentially freeze-dried to produce a highly porous, seamlessly integrated multi-layered scaffold, as demonstrated by scanning electron microscopy (extreme right), designed to mimic the composition and microstructural properties of the osteochondral region.
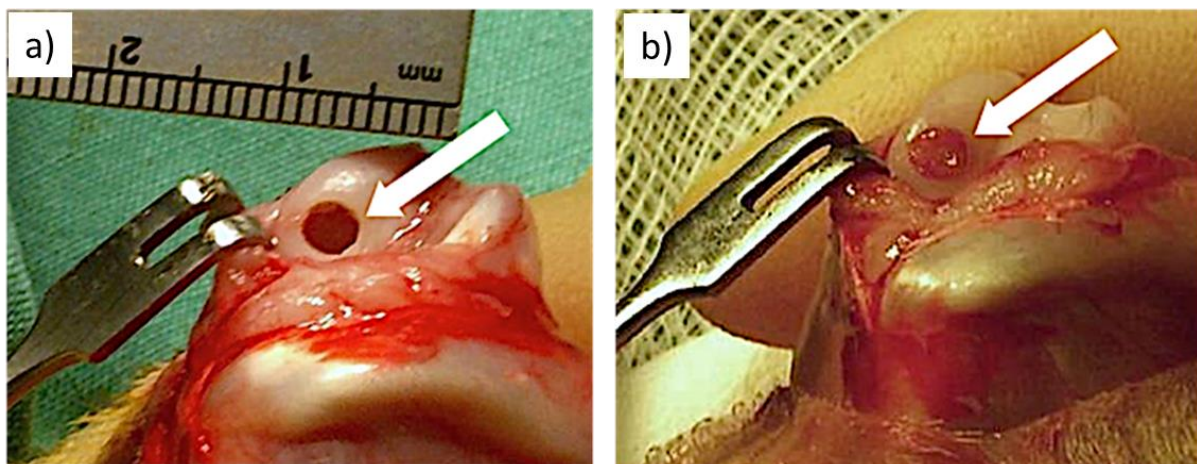

Figure 2: Multi-layered scaffolds were implanted into osteochondral defects (3 mm diameter x 5mm depth) created on medial femoral condyle. Intraoperative photographs show a) the size and location of the defect and b) Press-fit implantation of the multi-layered scaffold showing the close-fitting relationship between the implant and surrounding tissue.
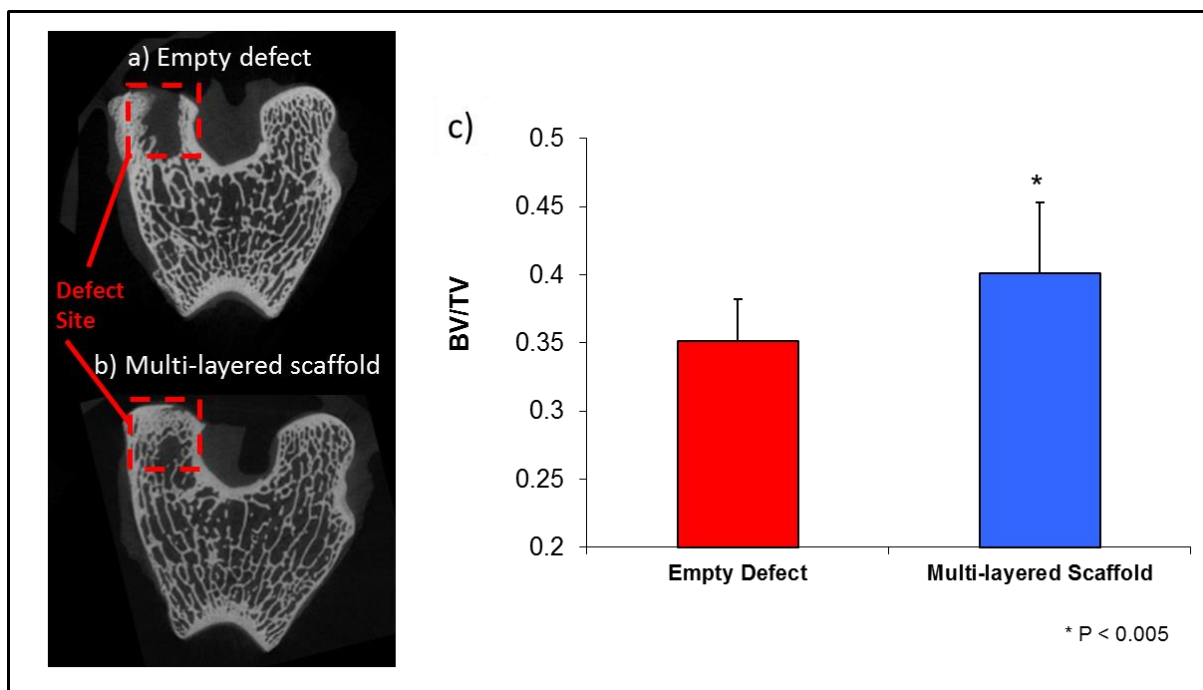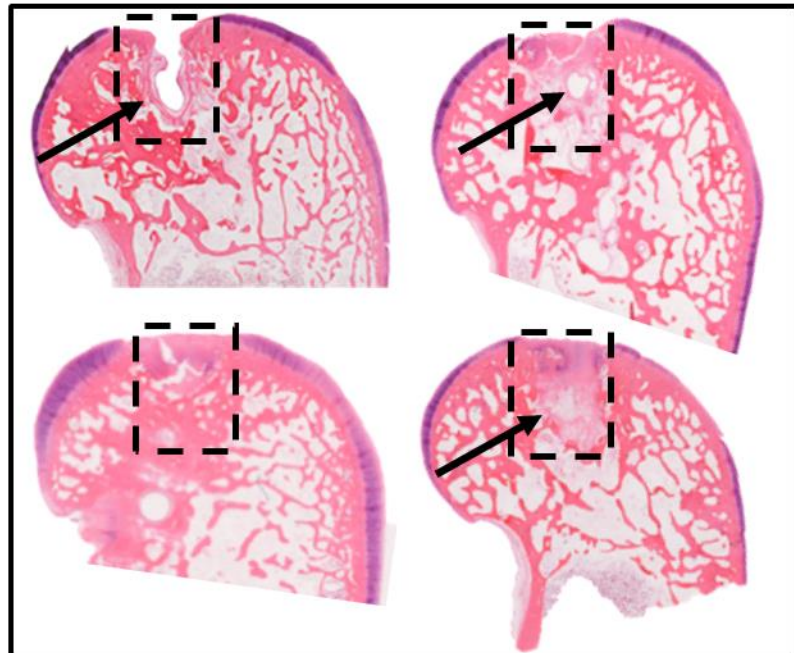
570

571 **Figure 3:** Improved macroscopic repair was observed in the multi-layer scaffold group
572 compared to the empty defect group at 12 weeks post implantation a) photograph showing
573 macroscopic appearance of the distal femur at 12 weeks post-surgery with neotissue
574 highlighted by the white circle b) Blinded quantitative macroscopic evaluation of repair tissue
575 formed in the empty defect and multi-layered scaffold groups by three investigators showed
576 that the multi-layered scaffold treated group had a higher average ICRS score compared to
577 controls. The values are expressed as mean ± standard deviation, n=4
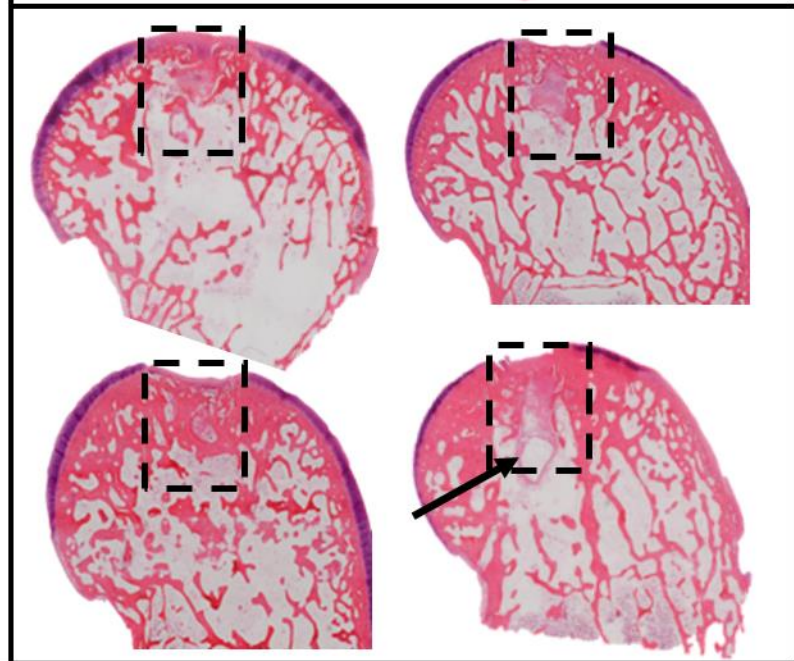

578

579   **Figure 4:** Micro-CT analysis at 12 weeks post-surgery showed greater levels of bone repair in

580   the multi-layered scaffold group than the empty defect group. 2D projection images show the

581   failure of subchondral bone restoration in the empty defect group (a). In comparison, the multi-

582   layered scaffold group (b) showed enhanced repair of subchondral bone after 12 weeks.

583   Quantitative micro-CT analysis of regenerated bone within the defect space of operated knees

584   demonstrates significantly greater level of bone formation in the multi-layered scaffold group

585   compared to the control group after 12 weeks in vivo (c). The values are expressed as mean $\pm$

586   standard deviation, n=4, *represents $p<0.05$ statistical significant differences relative to control

587   group.

588

Figure 5: H&E stained representative images from each animal show the region of the defect site and neotissue formed after 12 weeks in situ, highlighted with dashed lines. Slight depression of the superficial surface was noted in both groups with subchondral cysts occurring predominantly in the empty defect group (arrows).
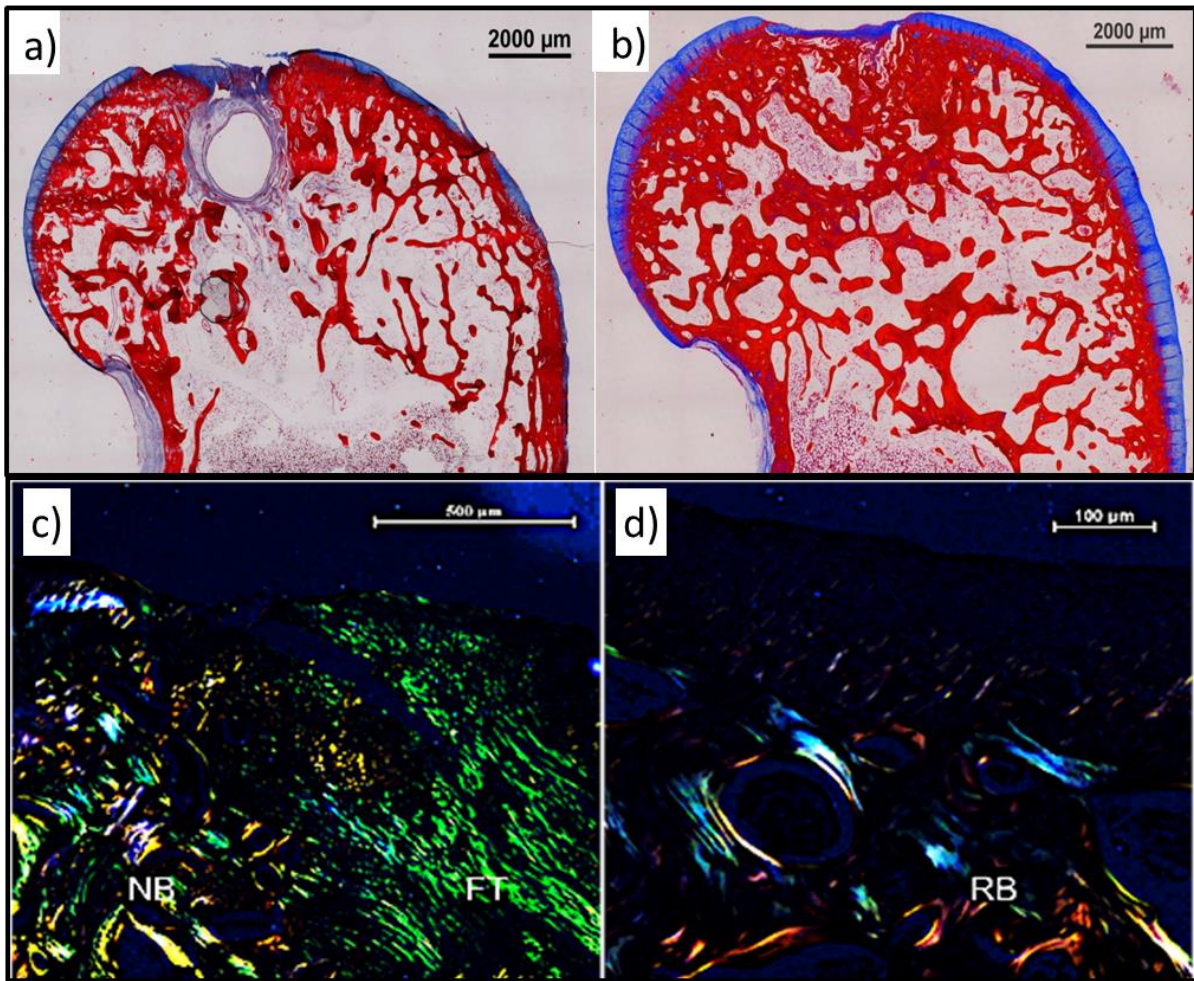
593

Figure 6: Masson's Trichrome stained images showing neo-tissue formation using bright-field (a,b) and polarised light (c,d,), in the empty defect (a,c) and multi-layered scaffold (b,d) groups at 12 weeks post-surgery –cartilage staining blue and bone staining red. Fibrous tissue with large residual void spaces within the subchondral bone region can be seen in the empty defect group (a). Multi-layered scaffolds displayed more advanced healing with regeneration of bone tissue within the subchondral bone and the formation of an overlying cartilage layer (b). Using polarised light microscopy, Fibrous tissue (FT) formation is seen in the empty defects (c) abutting native bone (NB). In contrast, multi-layered scaffolds (d) display regenerative bone (RB) adopting a concentric lamellar pattern of native subchondral bone.
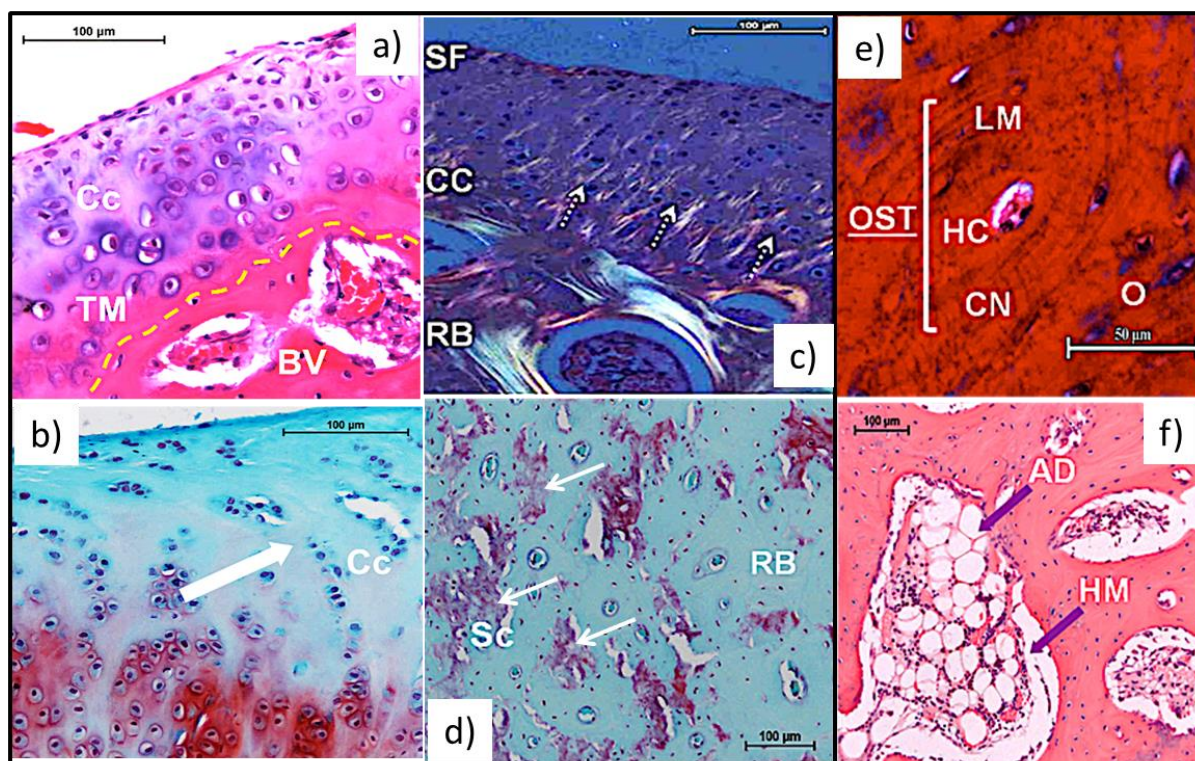
603

Figure 7: Histological analysis showed the formation of bone and cartilage within the defect site in the multi-layered scaffold group a) H&E stained histological image showing distinct cellular morphologies depending on location, transitioning from chondrocytes (Cc) to neovascularised subchondral bone (BV) with an intermediate basophilic tidemark (TM, highlighted in yellow). b) Safranin-O/fast green histological image showing cells (Cc) have adopted a hyaline-like cartilage arrangement with the production of sulphated glycosaminoglycans, staining red. c) Polarised light microscopy demonstrating the vertically orientation (white arrows) of collagen fibers in the transitional zone (CC) between superficial cartilage (SF) and regenerated bone (RB). d) H&E and Safranin-O/fast green image showing the presence of neo-tissue and some scaffold remnant (Sc: purple colour, highlighted with arrows) within the bone region with evidence of mature regenerated bone (RB: green) replacing the implanted scaffold. Qualitative Masson's trichrome (e) and H&E (f) histological image showing mature bone formation (e) with osteon (OST) formation including the presence of Haversian canals (HC), canaliculi (CN), osteocytes (O) and a lamellar bone pattern (LM) and

30

618   (f) restoration of the bone marrow cavity with highly cellularised regions resembling bone

619   marrow containing hemopoietic cells (HM) and adipocytes (AD) were seen between bony

620   trabeculae in the regenerated tissue adjacent to the host medullary cavity.

621

622   **Table 1**: International Cartilage Repair Society (ICRS) cartilage repair assessment tool. This

623   tool is used by surgeons to evaluate the macroscopic appearance of cartilage repair tissue

624   following interventions such as ACI, subchondral drilling and microfracture.

	Criteria	Points
Degree of Defect Repair	Level with surrounding cartilage 75% repair of defect depth 50% repair of defect depth 25% repair of defect depth 0% repair of defect depth	4 3 2 1 0
Integration to Border Zone	Complete integration with surrounding cartilage Demarcating border < 1mm 3/4 of graft integrated, 1/4 with a notable border >1mm width 1/2 of graft integrated with surrounding cartilage,1/2 with a notable border > 1mm From no contact to 1/4 of graft integrated with surrounding cartilage	4 3 2 1 0
Macroscopic Appearance	Intact smooth surface Fibrillated surface Small, scattered fissures or cracks Several, small or few but large fissures Total degeneration of grafted area	4 3 2 1 0
Overall Score	Grade I normal Grade II nearly normal Grade III abnormal Grade IV severely abnormal	12 11-8 7-4 3-1

625
626

627